Wideband Oscillations in Real-world Wide-Area Synchro-Waveforms: Onset Detection and Source Localization

Hossein Mohsenzadeh-Yazdi, *Student Member, IEEE*, David Daigle, Hamed Mohsenian-Rad, *Fellow, IEEE*

***Abstract*—A novel framework is proposed to detect, localize, and characterize wideband oscillations using real-world, low-voltage, wide-area *synchro-waveforms* from Waveform Measurement Units (WMUs). The proposed method relies solely on voltage waveforms. It does not require current measurements or network models. Oscillatory components are extracted, then band-pass filtered, and their Hilbert envelopes are computed to reveal amplitude modulation patterns. A novel metric based on the Iso-Amplitude Crossing Delay (IACD) is developed to determine the relative arrival times of the oscillations across WMUs, providing a robust estimate of both the onset time and the WMU closest to the oscillation source. The relative phase angles of the dominant mode are analyzed to distinguish between regional and inter-area oscillations. The proposed methodology accounts for practical challenges such as differing sampling rates and varying nominal voltages across WMUs. Two recent real-world events from the Western Interconnection in the United States are analyzed. Results show that the proposed approach accurately estimates onset times, identifies source proximity, and resolves closely spaced frequency components that cannot be captured by conventional PMU-based or long-window FFT methods. To the best of our knowledge, this is the first study to achieve voltage-only onset detection, source localization, and oscillation-type classification using real-world, wide-area synchro-waveforms.**

***Keywords*—Wideband oscillations, synchro-waveforms, waveform measurement unit, envelopes, onset detection, iso-amplitude crossing delay, time–frequency analysis, source localization.**

I. Introduction

Poorly damped oscillations in power systems are a critical class of network disturbance phenomena that cause unsafe mechanical vibrations in equipment, degraded power quality, instability, and uncontrolled outages [1]. Such oscillations can also excite network resonances, exacerbate harmonic and interharmonic conditions, and accelerate component wear, or even cause damage to various types of network apparatus. The severity and prevalence of such oscillatory disturbances have further intensified in recent years due to the increasing deployment of inverter-based resources (IBRs) [2].

Phasor Measurement Units (PMUs) have been widely used in recent years to detect and characterize oscillations or to identify their source locations. Various methods have been developed in this field, including admittance-matrix methods [3], statistical methods [4], time–frequency analysis [5], Fourier Synchrosqueezing Transform [6], multivariate variational mode decomposition [7], and SVM-based classifiers [8].

However, PMU measurements are inherently prone to errors when analyzing wideband oscillations, particularly when the oscillation frequencies are fractions of the fundamental frequency (sub-synchronous oscillations) or significantly higher than the fundamental frequency (high-frequency oscillations) [9]. Instead, *raw waveforms* from Waveform Measurement Units (WMUs) should be used, as recently discussed in [10]. This is because WMUs have higher sampling rates than PMUs, and provide the original voltage or current waveforms *without filtering out* information outside the fundamental frequency.

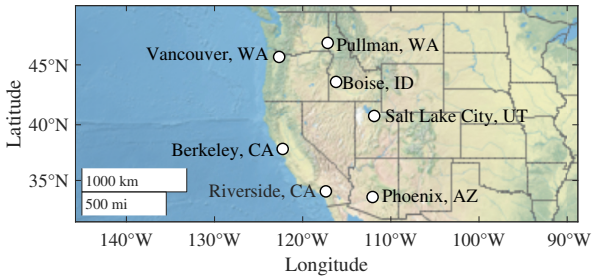

Fig. 1. Several WMUs are deployed[2] across the western United States to form a real-world wide-area synchro-waveform network for oscillation monitoring.

Methods that use WMU measurements have only recently begun to be developed. In [1] and [11], *both* voltage and current waveform measurements are used to identify sources of forced oscillations, and highlight components that degrade the damping of natural modes. However, the requirement to access not only voltage but also current waveforms at many locations poses a significant obstacle to adopting the above existing methodologies. It is also computationally burdensome.

Hence, in this paper, we seek to analyze wideband oscillations by using *solely* voltage waveform measurements from only a *few* sensor locations across the Western Interconnection in the United States; see Fig. 1. This is done by using *real-world* synchronized waveform measurements, also known as synchro-waveforms [10], from multiple WMU technologies.

The methods proposed in this paper can detect wideband oscillations, determine their onset-time, source locations, and frequencies, and distinguish between regional and inter-area oscillations using *only* voltage waveforms. Our real-world case studies demonstrate the effectiveness of using low-cost, wide-area synchro-waveforms to study wideband oscillations.

II. Problem Statement

Consider the network of WMUs shown in Fig. 1, spanning the Western Interconnection in the United States. The WMU in Riverside, CA, is a commercial-grade three-phase unit installed at a 480 V load transformer [13]. All other WMUs are single-phase units connected to standard 120 V power outlets [14]. Collectively, these WMUs provide a wide-area monitoring infrastructure for collecting synchro-waveforms.

H. M. Yazdi and H. Mohsenian-Rad (Corresponding Author) are with UC Riverside, USA. C. D. Daigle is with Daigle Grid Engineering LLC, USA.

[2]All the raw data for the studies in this paper are made available in [12].

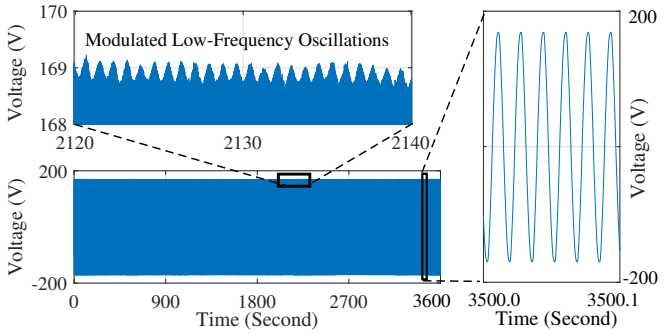

Fig. 2. A real-world example of voltage waveforms during wideband oscillations. Notice that the amplitudes of the sinusoidal waveforms fluctuate.

Fig. 2 shows the voltage waveforms from one WMU during a real-world low frequency oscillation event. The zoomed-in portions in the figure highlight the sinusoidal waveforms as well as the modulated low-frequency oscillations.

The available measurements consist of synchronized voltage waveforms $\{v_i[n]\}_{i=1}^m$ from m WMUs at m distinct locations. Let $\mathcal{A}_\Theta$ denote the oscillation-analysis algorithm with parameters Θ, such as thresholds, window sizes, weights, etc. Also, let f_0 denote the nominal grid frequency. We define:

$$\{d,\ i^\star,\ t_0,\ c\} \quad \leftarrow \quad \mathcal{A}_\Theta(\{v_i[n]\}_{i=1}^m;\ f_0)\,, \tag{1}$$

where we seek to identify the following unknowns:

- Oscillation detection indicator: $d \in \{0, 1\}$
- Nearest sensor-to-source proximity: $i^\star \in \{1, \ldots, m\}$
- Onset time: $t_0 \geq 0$
- Oscillation class: $c \in \{\text{Regional}, \text{Inter-Area}\}$.

Notably, low-voltage WMUs present several practical challenges. Nominal voltage levels as well as sampling rates can differ across WMUs. Time stamping schemes may also vary, e.g., GPS, NTP, or free-running clocks. In addition, *only voltage* waveforms are available from the WMUs in this study.

The method must account for the above limitations, *remain insensitive* to other event types, such as faults, switching, harmonics, and rely solely on voltage waveform data.

III. Methodology

Fig. 3 shows the overall flowchart of the proposed interrelated methodologies. Both amplitude and timing of the voltage waveforms play essential roles in this methodology. Note that voltage amplitude information can be distorted by the influence of local devices and local events, while timing information can be affected by errors in time stamping. By combining both amplitude and timing information, the methodology mitigates the challenges in either source of information; thus ensuring a *more robust* analytical framework.

A. Oscillation Detection and Dominant Mode Extraction

The first step in the methodology is a time–frequency analysis to detect wideband oscillations across sensor locations. Before computing the sliding-window FFT, the voltage waveforms are processed to track how the spectral content evolves over time. First, a suitable window length is selected. To reliably separate the fundamental frequency from each wideband component at frequency f_{wb}, the window must

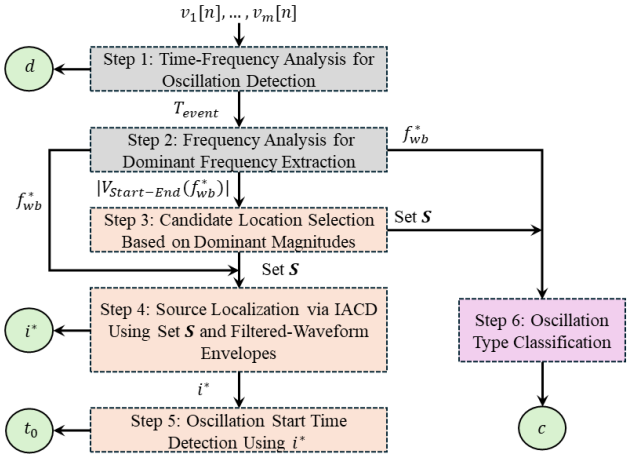

Fig. 3. Workflow of the proposed method. From voltage waveforms $v_1[n], \ldots, v_m[n]$, time-frequency analysis detects events (d, T_{event}), while frequency analysis gives f^*_{wb}. Filtering and Hilbert envelopes produce $e[n]$, followed by IACD to localize the source (i^*) and estimate onset t_0. In parallel, a phase-based step classifies the oscillation as inter-area or local (c).

span at least two cycles of the frequency separation $\Delta f = |f_0 - f_{wb}|$. Thus, the minimum number of samples per window, denoted by N_w, must satisfy:

$$N_w \ \geq 2f_s/|f_0 - \underline{f}_{wb}|, \tag{2}$$

where f_s is the sampling rate of the waveform measurements and $\underline{f}_{wb}$ is a user-defined parameter that denotes the minimum targeted wideband frequency for monitoring, and it is chosen based on application requirements (e.g., monitoring subsynchronous vs. near-fundamental low-frequency oscillations).

Now, the sliding-window FFT can be performed by using overlapping windows of length N_w and hop $H = \lfloor T_h f_s \rfloor$, where T_h is the hop duration in seconds. For window h, the discrete-time voltage segment is defined as

$$v_h \ = \ v[hH : hH + N_w - 1], \qquad h = 0, 1, \ldots \tag{3}$$

which is transformed via FFT as follow:

$$V_h(k) \ = \ \mathcal{F}\{\, v_h \,\}(k), \qquad k = 0, \ldots, k_{max}, \tag{4}$$

where $V_h(k)$ is the Fourier coefficient at frequency bin $f_k = kf_s/N_w$ for window h, $k_{max} = \lfloor \overline{f}_{wb} N_w/f_s \rfloor$, and $\overline{f}_{wb}$ is the maximum wideband frequency to be detected.

We can use $V_h(k)$ to estimate the start of oscillations. The oscillation event indicator for window h is defined as

$$d_h \ = \ \begin{cases} 1, & \exists\, k:\ f_k \in \mathcal{F}_{wb} \text{ and } |V_h(k)| > \eta_k, \\ 0, & \text{otherwise}, \end{cases} \tag{5}$$

where $\mathcal{F}_{wb} = [\underline{f}_{wb}, \overline{f}_{wb}]$, and η_k is a noise threshold at frequency bin f_k that is set based on the spectral magnitude during normal operation outside of the fundamental frequency.

Let N_{start} denote the index of the first window where the voltage spectrum exhibits magnitude above the baseline noise level within the target frequency interval $\mathcal{F}_{wb}$. Similarly, let N_{end} denote the last window during which the wideband oscillation is present. Given N_{start} and N_{end}, the duration of the oscillation event is approximated by $T_{\text{event}} \ \approx \ (N_{\text{end}} - N_{\text{start}})\, T_h$,

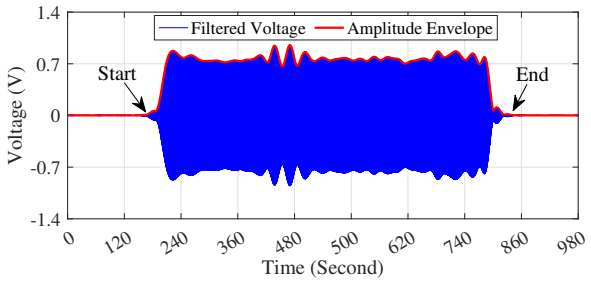

Fig. 4. A real-world example of filtered voltage (blue) and its amplitude envelope (red). The start and end of oscillation event are marked.

A global detection flag is defined as $d = 1$ when $T_{\text{event}} > 0$, and $d = 0$ when $T_{\text{event}} = 0$. An oscillation event is declared if the estimated duration is strictly positive, i.e., when more than one window within $\mathcal{F}_{wb}$ exceeds the noise threshold η_k.

The frequency of the *dominant* component of the wideband oscillations can be estimated as:

$$f_{wb}^{*} = \arg\max_{f \in \mathcal{F}_{wb}} |V_{\text{Start-End}}(f)|, \tag{6}$$

where $V_{\text{Start-End}}(f)$ is the resulting frequency spectrum of applying FFT to the concatenated signal segment spanning from window N_{start} through window N_{end}. From (6), the magnitude of the dominant component is obtained as $|V_{\text{Start-End}}(f_{wb}^{*})|$.

B. Source Localization and Onset Time Detection

Candidate Location Selection: To enable fair comparison across locations with different nominal voltage levels, we normalize the results in (6) by the WMU's nominal voltage. If the resulting oscillation magnitude exceeds a minimum threshold (e.g., 10% of the maximum observed magnitude), the corresponding location is retained as a *candidate* location, since it is more likely to be close to the oscillation source. Therefore, the candidate set $\mathcal{S}$ is defined as

$$\mathcal{S} = \left\{ i \mid g_i \geq \alpha \cdot \max_k g_k \right\}. \tag{7}$$

where g_i is the normalized dominant oscillation magnitude at WMU i, and α is the relative magnitude threshold.

Source Localization via IACD: The key criterion for locating the closest WMU to the oscillation source is the arrival time: the earlier a WMU registers the oscillation onset, the closer it is presumed to the source. Thus, access to time-synchronized waveforms is necessary in this analysis. To quantify this, the Iso-Amplitude Crossing Delay (IACD) method is employed.

Remember the frequency of the dominant component f_{wb}^{*} is obtained from (6). Around the identified dominant frequency, a band-pass filter centered at f_{wb}^{*} with bandwidth $\pm f_f$ is applied to extract the oscillatory component with the following band:

$$\mathcal{F}_{\text{pass}} = [f_{wb}^{*} - f_f, f_{wb}^{*} + f_f]. \tag{8}$$

Let $v_{wb}[n]$ denote the band-pass filtered signal of the original waveform $v[n]$ from the candidate location set. Using Hilbert transform $\mathcal{H}\{\cdot\}$, the oscillation envelope is obtained as:

$$e[n] = \sqrt{v_{wb}^2[n] + \left(\mathcal{H}\left\{v_{wb}[n]\right\}\right)^2}, \tag{9}$$

A real-world example of the envelope is shown in Fig. 4.

In the first step of IACD, envelopes are normalized to make their amplitudes comparable across different WMUs:

$$e_{\text{norm}}[n] = \frac{e[n] - \text{median}(e)}{q_{0.95}(e) - \text{median}(e)}, \tag{10}$$

where $q_{0.95}(e)$ is the 95th percentile of $e[n]$. This centers each envelope at its median and scales it by the 95th–median range.

For two normalized envelopes $e_i[n]$ and $e_j[n]$, define a set of iso-amplitude levels, i.e., amplitude values at which both envelopes are compared, typically selected from the early portion of the rising edge during the onset:

$$\mathcal{L} = \{l_1, l_2, \ldots, l_{max}\}, \quad l_{max} \leq 1.0, \tag{11}$$

For each $l_q \in \mathcal{L}$, the first sustained up-crossing time, i.e., when the envelope first rises above l_q, is detected:

$$t_i(l_q) = \inf\{t : e_i(t) \geq l_q \text{ for at least } \tau_s\}, \tag{12}$$

where τ_s is a hysteresis parameter to avoid spurious crossings.

The IACD delay estimate between WMU i and WMU j is the median across all levels of per-level pairwise delays:

$$\Delta_{ij} = \text{median}_{q \in \{1,\ldots,max\}} \Delta_q(i,j). \tag{13}$$

Using the estimated pairwise delays, the closest WMU to the oscillation source is identified as the WMU that minimizes the overall delay to all other candidate locations:

$$i^{*} = \arg\min_{i \in S} \sum_{j \in S \setminus \{i\}} |\Delta_{ij}|. \tag{14}$$

Oscillation Onset: Once the closest WMU to the source is identified, i.e., the WMU with the earliest onset, the global oscillation start time is estimated as $t_0 \approx t_{i^*}(l_1)$. For all other WMUs j, the estimated start time is given by $t_j(l_1)$, which provides a synchronized onset across WMUs.

C. Oscillation Type Classification

If an oscillation exhibits large magnitudes across multiple WMUs, it may indicate a system-wide *inter-area* oscillation, characterized by power exchange across regions. Such oscillations can be distinguished from oscillations that affect only one region by comparing the phase angles of the dominant mode across WMUs, which typically form region-wise clusters [15].

First, the instantaneous phase at each WMU is calculated. For WMU i, the analytic signal is formed using the Hilbert transform, $a_i[n] = v_i[n] + j\,\mathcal{H}\{v_i[n]\}$, whose angle gives the instantaneous phase, $\phi_i[n] = \text{unwrap}(\arg a_i[n])$.

Next, the system frequency f_0, which can be estimated from the voltage waveform to account for slight off-nominal frequency deviations, is removed from each waveform. The instantaneous phase is expressed as $\phi_i[n] \approx 2\pi f_0\,(n/f_s) + \delta_i[n]$, where $\delta_i[n]$ is the deviation from the nominal carrier. Subtracting the first term isolates this deviation.

Finally, an FFT is applied to $\delta_i[n]$ over a time-synchronized window. At the known dominant oscillation frequency $f_m = |f_{wb}^{*} - f_0|$, the FFT coefficient $C_i = Y_i(f_m)$ is extracted, and the oscillation phase angle is obtained as $\theta_i = \arg(C_i)$. The results are then compared with a common reference to obtain the *relative* phase angles to capture the spatial differences.

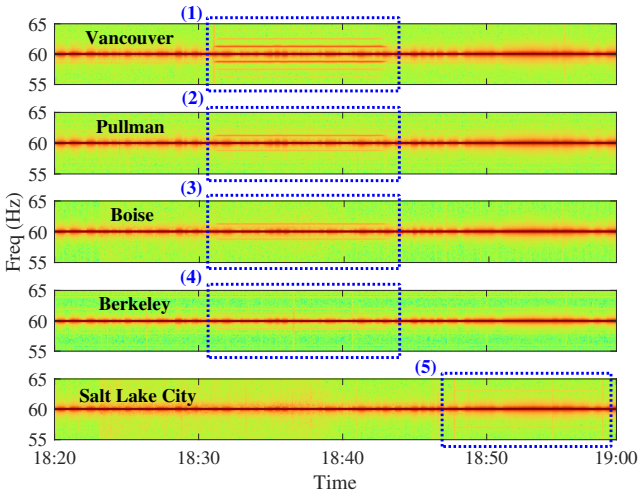

Fig. 5. Spectrograms of voltage waveforms during Case Study 1.

If the phase angles within one region are nearly identical (thus oscillating together), while differing from those in other regions, the oscillation is classified as *inter-area*. Such inter-area modes typically have frequencies below 1 Hz [16, pp. 55].

IV. Experimental Results

A. Case Study 1: November 30, 2024

On November 30, 2024, an oscillation event affected Northwest United States. At 18:31, the PACW Merwin–Cherry Grove 115 kV line tripped due to a fault, which immediately tripped Merwin Hydro Unit 3 offline. Between 18:31 and 18:43, multiple nearby units exhibited active-power fluctuations. At 18:43, the PACW generation operator shut down both Yale hydro units, after which the system stabilized [17].

Voltage waveforms were recorded during the event at five locations, all at 120 V power outlets: Vancouver WA, Pullman WA, Boise ID, Salt Lake City UT, and Berkeley CA. The sampling rate is 4 kHz, i.e., 4,000 data samples per second.

The time–frequency spectrograms of the voltage waveform measurements are shown in Fig. 5. Highlighted intervals (1)–(4) at the first four WMUs indicate time ranges where wideband oscillations are observed, showing higher magnitudes in Vancouver and lower magnitudes in Berkeley. The highlighted interval (5) marks the time range where a wideband oscillation is observed in Salt Lake City.

To extract the principal oscillation frequencies, a frequency analysis is performed over the event duration identified by the above time–frequency analysis. Fig. 6 shows the magnitude spectra of voltage waveforms for the window from 18:31 to 18:44, at the four locations where the oscillation was observed. The dominant wideband components appear at 58.7724 Hz and 61.2236 Hz. Additional frequency components at 57.5462 Hz and 62.4498 Hz are observed only in Vancouver.

Based on the dominant frequency, a band-pass filter is designed to isolate the oscillatory voltage component. For this case, the passband is centered at 61.22 Hz with a half-bandwidth of 0.05 Hz (i.e., 61.17–61.27 Hz).

Three locations were selected in the first phase of the source-localization methodology. The magnitude of the dominant component at the weakest WMU (Boise) exceeds 10% of the maximum among the three WMUs (Vancouver), satisfying the candidate-selection criteria in Section III.B.

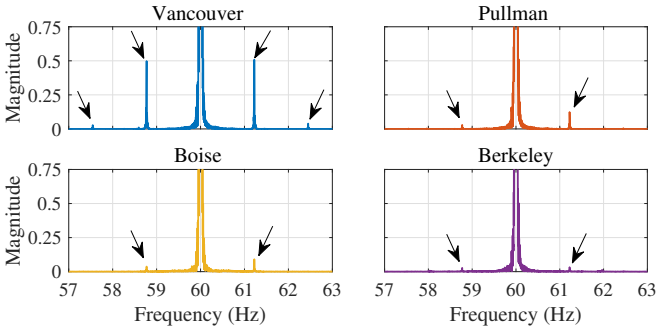

Fig. 6. Magnitude spectra of voltage for time window 18:31 – 18:44 from four WMUs in Northwest United States. Arrows mark sideband peaks.

TABLE I
Pairwise IACD results for estimating delays Δt, 95% confidence intervals, and the leading WMU for each pair.

Pair	Δt (s)	95% CI (s)	Leader
Vancouver–Pullman	0.096	[0.018, 0.511]	Vancouver
Vancouver–Boise	1.4835	[0.568, 3.5548]	Vancouver
Pullman–Boise	1.5079	[0.543, 3.313]	Pullman

In the second phase of source localization, the key indicator is the moment when the filtered waveform envelope begins to rise. These rise-onset moments are compared pairwise to identify the WMU closest to the oscillation source.

The results of the pairwise IACD analysis are shown in Table I. Accordingly, the WMU in Vancouver is identified as the closest to the oscillation source. The WMU in Pullman is also closer to the source compared to the WMU in Boise.

Since the closest WMU to the oscillation source is in Vancouver, it is used for start-time detection. According to the IACD results at this location, the normalized envelope exceeds 0.1 at 18:31:07, indicating the event onset.

Since only one WMU (in Vancouver) observed the dominant oscillation mode with significant magnitude, the oscillation is classified as *regional*, affecting only a small region.

B. Case Study 2: March 11, 2025

Brief but significant forced oscillations occurred on March 11, 2025. These oscillations were observed over a wide area, from Riverside, CA in the south to Vancouver, WA in the north. Recall that the WMU in Riverside is three-phase with a sampling rate of 3 kHz, whereas the WMU in Vancouver is single-phase with a sampling rate of 8 kHz. This section examines how these two WMUs perceived the oscillations and evaluates the ability of the proposed method to detect and characterize them, in comparison with the method in [18].

The method in [18] addresses the broader problem of anomaly analysis in waveform measurements, where oscillations are modeled as one class of anomaly. To enhance sensitivity to low-frequency oscillations amid small cycle-by-cycle variations, the approach in [18] fits a quadratic function to the instantaneous phase extracted from the voltage waveform; thus isolating frequency deviations from the fundamental component. A 5-second FFT is then applied to this frequency trace to obtain the power spectral density (PSD), which is used to detect and characterize the superposed oscillations.

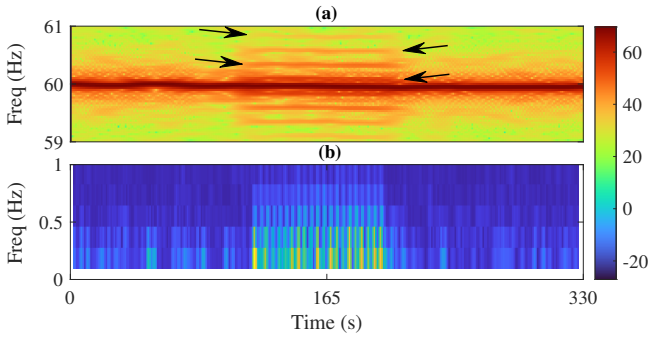

Fig. 7. Frequency spectrum in Case Study 2, based on different methods: (a) The proposed method in this paper; (b) The method in [18].

TABLE II
RPAD AT $f_m = 0.123$ HZ IN CASE STUDY 2.

City	Relative Phase (°)	City	Relative Phase (°)
Salt Lake City	0.000	Berkeley	5.257
Boise	-3.749	Vancouver	5.247
Pullman	-2.295	Riverside	12.174

Figs. 7(a) and (b) show the frequency spectra of the voltage waveforms from the WMU in Riverside before, during, and after the oscillations, obtained using the proposed method and the method in [18], respectively. The proposed approach clearly resolves the sideband components, as indicated by the arrows. In contrast, while the method in [18] can detect the presence of oscillatory components, it struggles to accurately identify their frequencies. Because the 5-second FFT used in [18] fixes the resolution at $\Delta f \approx 1/T = 0.2$ Hz (with leakage), very low-frequency modulations (e.g., ~ 0.1 Hz) and closely spaced sidebands appear blurred. Moreover, the proposed method operates directly on time-aligned raw voltage waveforms, without intermediate instantaneous phase or frequency estimation, reducing computational cost. The method in [18], however, is designed for general anomaly detection on a broader range of events in both time and frequency domains.

Fig. 8(a) shows the magnitude spectra of voltage waveforms from Riverside (three-phase) and Vancouver (single-phase). Two pairs of wideband oscillations are visible. The dominant-frequency magnitudes are nearly equal across all three phases at Riverside, indicating a balanced oscillation. Fig. 8(b) shows the voltage envelopes from these two GPS-synchronized WMUs. Although the envelope magnitudes differ, the rise times are similar, suggesting a common onset.

Table II shows the phase angle differences of the dominant oscillation mode, referenced to the WMU in Salt Lake City. There are three groups of similar phase angles at each region, such as at Boise and Pullman, as well as at Berkeley and Vancouver; while the phase angle is different in Riverside in Southern California. This suggests an inter-area oscillation. It is worth noting that California Independent System Operator (ISO) also labeled this event as an inter-area oscillation [17].

V. CONCLUSIONS AND FUTURE WORK

This paper presented a voltage-only framework for detecting, localizing, and classifying wideband oscillations from real-world, wide-area synchro-waveforms. Case studies from the Western Interconnection demonstrate accurate onset estimation, reliable source localization, and clear resolution of

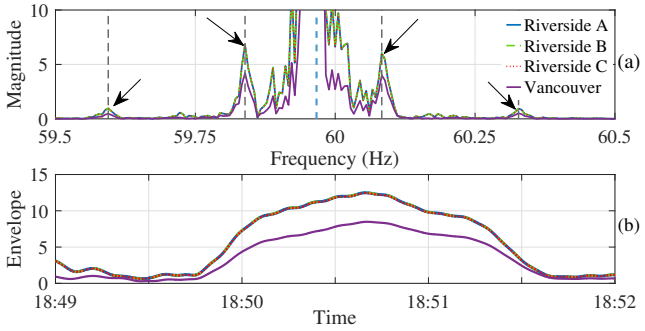

Fig. 8. Spectral magnitude of the voltage waveforms at different WMUs in Case Study 2, and their corresponding oscillation envelopes of the filtered waveforms (60.07-60.1 Hz) in the time domain showing balanced oscillations.

closely spaced sidebands that are blurred in long-window FFT baselines. Given the low-voltage nature of the measurements (120 V and 480 V), the approach provides an effective and low-cost means of enhancing situational awareness.

Future work may include also using measurements from PMUs or limited high-voltage WMUs; developing automated alarms for operators, and enabling online deployment with adaptive parameter learning and uncertainty quantification.

REFERENCES

[1] P. G. Estevez and S. Maslennikov, "Extension of the complex dissipating energy flow method for sub/super-synchronous oscillation source location," *IEEE Trans. on Power Systems*, pp. 1–12, 2025.
[2] N. Modi *et al.*, "Replication of real-world sub-synchronous oscillations in inverter-based resources dominated grid," *IEEE Trans. on Power Delivery*, vol. 39, no. 3, pp. 1399–1406, 2024.
[3] S. C. Chevalier, P. Vorobev, and K. Turitsyn, "Using effective generator impedance for forced oscillation source location," *IEEE Trans. on Power Systems*, vol. 33, no. 6, pp. 6264–6277, 2018.
[4] S. Chevalier, P. Vorobev, and K. Turitsyn, "A bayesian approach to forced oscillation source location given uncertain generator parameters," *IEEE Trans. on Power Systems*, vol. 34, no. 2, pp. 1641–1649, 2018.
[5] P. G. Estevez, P. Marchi, F. Messina, and C. Galarza, "Forced oscillation identification and filtering from multi-channel time-frequency representation," *IEEE Trans. on Power Systems*, vol. 38, pp. 1257–1269, 2022.
[6] P. G. Estevez, P. Marchi, C. Galarza, and M. Elizondo, "Non-stationary power system forced oscillation analysis using synchrosqueezing transform," *IEEE Trans. on Power Systems*, vol. 36, pp. 1583–1593, 2020.
[7] T. Jiang, B. Liu, B. Wang, G. Liu, and X. Li, "Forced oscillation source location in power systems using mvmd-assisted def in tf plane," *IEEE Trans. on Power Systems*, vol. 39, no. 6, pp. 6901–6913, 2024.
[8] H. Liu, Y. Qi, J. Zhao, and T. Bi, "Data-driven subsynchronous oscillation identification using field synchrophasor measurements," *IEEE Trans. on power delivery*, vol. 37, no. 1, pp. 165–175, 2021.
[9] B. Gao, Y. Wang, W. Xu, and G. Yang, "Identifying and ranking sources of ssr based on the concept of subsynchronous power," *IEEE Trans. on Power Delivery*, vol. 35, no. 1, pp. 258–268, 2020.
[10] H. Mohsenian-Rad and W. Xu, "Synchro-waveforms: A window to the future of power systems data analytics," *IEEE Power and Energy Magazine*, vol. 21, no. 5, pp. 68–77, 2023.
[11] W. Xu, J. Yong, H. J. Marquez, and C. Li, "Interharmonic power–a new concept for power system oscillation source location," *IEEE Trans. on Power Systems*, vol. 40, no. 5, pp. 4367–4379, 2025.
[12] "Raw oscillation and measurement data for this study," data repository.
[13] [Online]. Available: https://selinc.com/products/2240/
[14] [Online]. Available: https://kestrelgrid.com/
[15] I. Idehen, B. Wang, K. Shetye, T. Overbye, and J. Weber, "Visualization of large-scale electric grid oscillation modes," in *IEEE NAPS*, 2018.
[16] H. Mohsenian-Rad, *Smart Grid Sensors: Principles and Applications*. Cambridge University Press, UK, Apr. 2022.
[17] D. Daigle from California ISO, "Inverter-Based Generation and Loads — Challenges and Opportunities — Part 1," in *IEEE PES General Meeting*, Austin, TX, July 2025, Panel Presentation.
[18] H. Yin *et al.*, "Anomaly identification of synchronized voltage waveform for situational awareness of low inertia systems," *IEEE Trans. on Smart Grid*, vol. 16, no. 3, pp. 2416–2428, May 2025.